Chaos in one-dimensional collision complexes

1991 J. Phys. A: Math. Gen. 24 153

(http://iopscience.iop.org/0305-4470/24/1/024)

J. Phys. A: Math. Gen. **24** (1991) 153–173. Printed in the UK

Chaos in one-dimensional collision complexes

P Eckelt and E Zienicke

Institut für Theoretische Physik I der Universität Münster, D-4400 Münster, Federal Republic of Germany

Received 15 August 1990

Abstract. The classical scattering of a particle by an oscillating potential well is investigated. It is shown that the singularities of the scattering map S form a Cantor set for this system. This result is obtained from an analysis of the particle's return map, which contains a Smale's horseshoe and, consequently, a hyperbolic invariant set with chaotic dynamics. The Cantor set structure of the S-singularities involves arbitrarily complex scattering behaviour.

1. Introduction

Chaotic scattering (also termed 'irregular scattering', see the recent review by Eckhardt [1]) in the framework of classical mechanics was first observed numerically in atom–molecule collisions [2–4]. It has also been found in potential scattering [5–8], in gravitational three-body problems [9], in hydrodynamical vortex scattering [10, 11] and in the scattering of a charged particle by a magnetic dipole field [12]. The essential feature of chaotic scattering is a Cantor set of singularities in the scattering map. This singularity structure implies highly sensitive dependence of the final scattering state on the initial conditions.

For the explanation of irregular scattering Jung and Scholz proposed the following line of argument (see [8, 12]). In the phase space of a system exhibiting chaotic scattering there is a hyperbolic invariant set consisting of an uncountable infinity of periodic and aperiodic orbits. Their stable and unstable manifolds extend to the asymptotic region by means of the Hamiltonian flow. If the projectile enters the region of interaction along such a stable manifold, it will be captured by the target on the corresponding orbit, thus leading to a singularity in the scattering map. In this way the set of unstable orbits in the interaction region causes a corresponding fractal set of scattering singularities. This conception about the origination of irregular scattering has been tested on some model systems and meanwhile is commonly accepted (see [1]).

Since a fractal implies a self-similar structure, thereby giving its own rule of construction, the following question is of interest. In what way is the self-similar structure and the corresponding rule of construction connected with the dynamics of the hyperbolic invariant set? According to the description given above the fractal structure of the scattering data should be an image of the dynamics of the hyperbolic set via the Hamiltonian flow. But only in a few cases can the construction rule of a fractal that one finds in the scattering of a system be cleared up (see e.g. [12]). Answering the above question is much easier if it is possible to describe the dynamics of the hyperbolic

0305-4470/91/010153+21$03.50

set in terms of symbolic dynamics. The symbolic dynamics has a direct connection to the dynamics of the scattering system and, beyond it, gives the construction rule for the fractal. Up to now, the symbolic dynamics has only been found for a few rather simple scattering systems (see [8, 13, 14]).

In this paper we introduce a class of systems for which a hyperbolic invariant set and its symbolic dynamics were found by Alekseev [15–18]. The class of systems consists of one-dimensional oscillating potential wells. It differs from the models of [8, 13, 14] by its time dependence and by the fact that the dynamical alphabet has an infinite number of symbols. In addition, it seems to have some relevance for the description of atomic and molecular scattering processes. We remark that the special case of the restricted three-body problem considered by Sitnikov ([19], see also [20]) is a member of this potential class. It is also mentioned in [1] as a candidate for chaotic scattering.

In the following we will verify in full detail for this class of systems the mechanism of the origination of chaotic scattering described above. In addition, the symbolic dynamics of the hyperbolic invariant set will enable us to expose the organizational structure of the fractal of scattering singularities and to clear up its connection with the dynamics of the system. We proceed as follows. In section 2 we verify chaotic scattering and determine its structure with the help of some numerical experiments for a representative of our potential class. In section 3 we analyze the formation of a horseshoe. The corresponding symbolic dynamics can be extended to the description of scattering motion with the help of finite symbol sequences. The results of this section are mainly due to Alekseev. For our purpose, which is the understanding of the scattering behaviour, it seemed to us that a detailed summary of Alekseev's work giving us insight into the behaviour of the system was necessary. Additionally, we want to make these results more widely known for their connection with chaotic scattering. (The review [1] only mentions a theorem of Sitnikov for the restricted three-body system, but not the more general results of Alekseev.) Since the statements of section 3 are only of a local nature we have to extend them to a global scale in section 4, where we come to the explanation of the structures which we found numerically in section 2.

2. The model and numerical results

We want to study the classical scattering of a particle by a one-dimensional oscillating potential well. We assume the potential $V(x,t)$ to be *symmetric* and *attractive* with respect to the origin for all times t. The dynamics of the particle (mass $m = 1$) is governed by Newston's equation of motion:

$$\ddot{x} = -\frac{\partial}{\partial x} V(x,t). \tag{1}$$

Our system is a Hamiltonian system with the Hamilton function

$$H(x,p,t) = \tfrac{1}{2}p^2 + V(x,t). \tag{2}$$

To be sure of the existence of a horseshoe in the dynamics of (1) $V(x,t)$ has (besides being symmetric and attractive) to fulfil some additional restrictions which can be found in [16] and [18].

As a representative of the admitted potentials we chose

$$V(x,t) = -\frac{1}{x^2+1} - \epsilon\frac{\cos t}{(x^2+1)^{5/2}} \tag{3}$$

for numerical calculations of the scattering map. The asymptotic behaviour ($\sim |x|^{-2}$) for $|x| \to \infty$ is given by the first term. The second term introduces the time dependence with a period $T = 2\pi$. The perturbation parameter ϵ controls the strength of the time-dependent part of the potential.

To compute the scattering map S—mapping initial states to final states—we have to introduce appropriate dynamical variables which become constant asymptotically and serve to label the initial and final states. We propose to characterize the free motion of the particle by its kinetic energy E and by its time of impact τ, i.e. the instant of crossing the origin. These two variables are connected with the canonical pair (x,p) by the time-dependent canonical transformation

$$T_t : (x,p) \to (E,\tau) \qquad E = \tfrac{1}{2}p^2 \qquad \tau = t - \frac{x}{p}. \tag{4}$$

This transformation is valid if

$$\lim_{|x|\to\infty} |x|V(x,t) = 0 \tag{5}$$

i.e. the asymptotic motion of the particle is given by free motion. In the case of a Coulomb asymptotic ($V(x,t) \sim |x|^{-1}$ for $|x| \to \infty$) one would have to change the definition of τ, because the particle never becomes free in a Coulomb potential due to its long range.

Denoting the flow of the Hamiltonian system (2) by

$$\Phi_{t't} : (x(t),p(t)) \to (x(t'),p(t')) \tag{6}$$

we get the scattering map (see also [21]) to be

$$S = \lim_{t'\to+\infty} \lim_{t\to-\infty} T_{t'} \circ \Phi_{t't} \circ T_t^{-1}. \tag{7}$$

This operator maps the incoming pair (E,τ) onto the outgoing pair (E',τ') of the particle. As a composition of canonical transformations S itself is a canonical transformation.

We computed S for potential (3) with $\epsilon = 0.1$. (What happens when ϵ is varied will be shown at the end of this paper.) First we held τ fixed at the value $\tau = \pi$. Then the final asymptote characterized by (E',τ') is a function only of the initial energy E. Instead of E' and τ' we plotted the 'inelasticity' $\Delta E = E' - E$ and the 'time delay' $\Delta\tau = \tau' - \tau$ in figures 1–4. As additional information we plotted the number N of times the particle passes the origin $x = 0$. $N - 1$ is the number of times the particle changes its direction of motion.

In figure 1 we present the results for the energy interval $[0.000, 0.075]$. One realizes a sequence of intervals accumulating against the energy $E = 0$ on which ΔE and $\Delta\tau$ are smooth functions of E. Between these intervals there are gaps in which the values of ΔE and $\Delta\tau$ seem to jump in an irregular way. The intervals belong to trajectories with exactly one zero (no turning point), as one can see in the third diagram of figure 1,

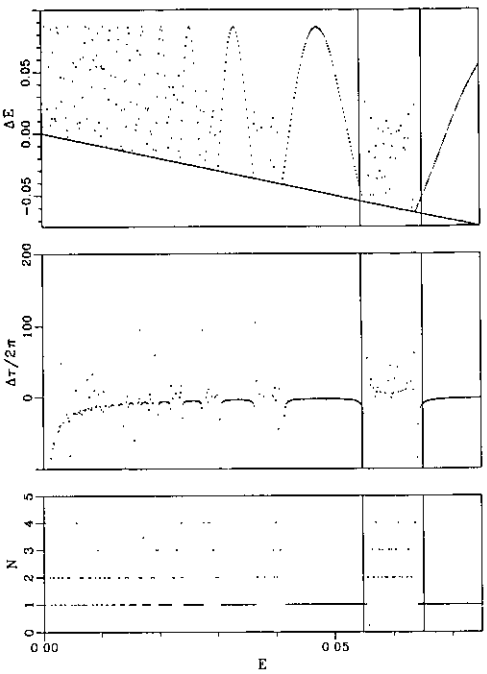

Figure 1. Inelasticity ΔE, time delay $\Delta\tau$ and the number of zeros N as functions of the incoming energy E. The unit of energy corresponds to the mean potential depth. Note $\Delta E \geq -E$. The marked interval is magnified in figure 2. $\epsilon = 0.1$.

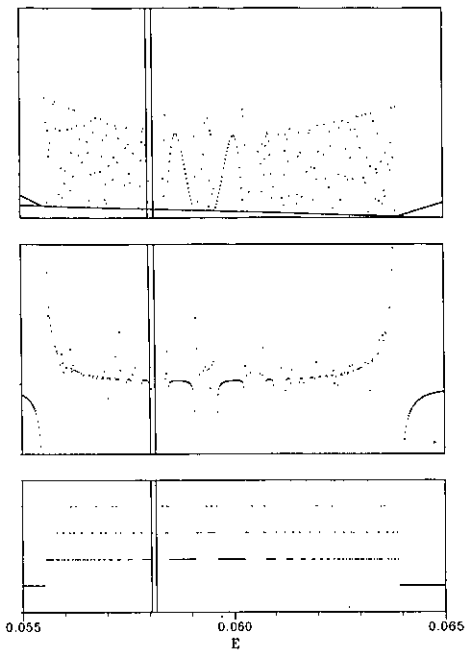

Figure 2. Magnification of the E interval indicated in figure 1. The marked interval is magnified in figure 3. The vertical axis has the same scale as figure 1.

where N is plotted against E. In the gaps the corresponding trajectories have two or more zeros. The straight line in the diagram ΔE against E corresponds to $E' = 0$. The area under this line is forbidden, because E' must be greater than or equal to zero. For $E' \to 0$, i.e. $\Delta E \to -E$ we have $\tau' \to -\infty$, i.e. $\Delta\tau \to -\infty$, as one can see from the transformation (4). In the following text we will call escape orbits with $E' = 0$ *parabolic* and escape orbits with $E' > 0$ *hyperbolic*.

Figure 2 shows a magnification of the gap marked in figure 1. The irregular behaviour of the values of ΔE and $\Delta\tau$ in figure 1 dissolves into a new series of intervals on which ΔE and $\Delta\tau$ are smooth functions of the initial energy. The intervals accumulate against the boundaries of intervals with $N = 1$ enclosing the gap. As can be seen from the third diagram the intervals belong to trajectories which pass the origin $x = 0$ twice and change its direction of motion along the x axis once. Between the intervals there are gaps in which the values of ΔE and $\Delta\tau$ seem to be distributed in an irregular way.

The next figure (figure 3) shows a magnification of the left part of one of these gaps. Here we find the same structure of intervals with $N = 3$. In the gaps we have $N \geq 4$. Here we made a magnification of the right part of one of the gaps and again found the same structure, one level higher in N (figure 4).

In summary, we found the following self-similar structure: in the gap between two N intervals (i.e. intervals belonging to solutions with N zeros) one finds an infinity of

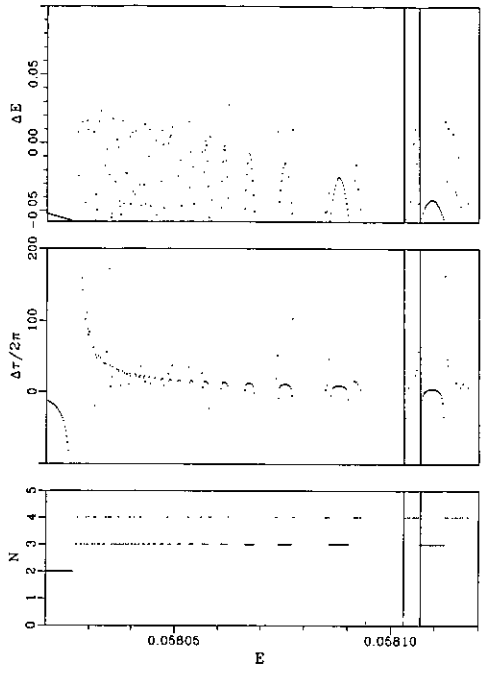

Figure 3. Magnification of the E interval indicated in figure 2. The marked interval is magnified in figure 4.

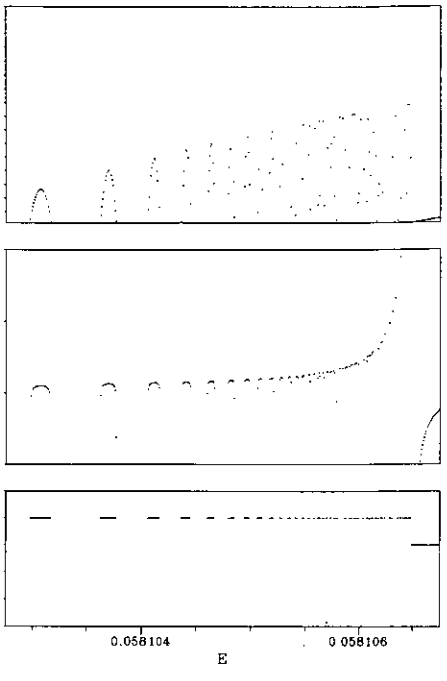

Figure 4. Magnification of the E interval indicated in figure 3. The vertical axis has the same scale as figure 3.

$(N+1)$ intervals on which ΔE and $\Delta\tau$ are smooth and which converge against the boundaries of the enclosing N intervals. The number N of zeros of the solutions plays the role of an order parameter marking the level of the observed self-similar structure. The smooth intervals become open intervals when we exclude their boundaries, which correspond to parabolic escape ($E' = 0$). Successive removal of all the smooth open intervals with $N = 1, 2, 3 \ldots$ leads to a Cantor set of singularities of the scattering map consisting of the initial conditions with out-asymptote $E' = 0$ and initial conditions without out-asymptote (capture orbits).

According to our results the scattering map is continuous where N is constant, and discontinuous where N changes its value. Therefore it is desirable to know the shape and the distributions of the sets

$$C_n = \{(E, \tau) | n = N - 1\} \tag{8}$$

in the (E, τ) plane. This leads to our next numerical experiment. We computed C_1, the set of all scattering initial conditions whose corresponding trajectories have exactly two zeros, in the (E, τ) plane. We restricted τ to the interval $[0, 2\pi)$ because of the 2π periodicity of the potential oscillations. We divided the E interval $[0.03, 0.09]$ and the τ interval into 500 and 400 equidistant points, respectively. Each of these 200 000 initial conditions was integrated numerically until it could be decided, whether the corresponding solution possessed $N = 1$, $N = 2$ or $N \geq 3$ zeros. For all trajectories with $N = 2$ we marked the corresponding (E, τ) by a dot, thus obtaining C_1. The result of this procedure can be seen in figure 5.

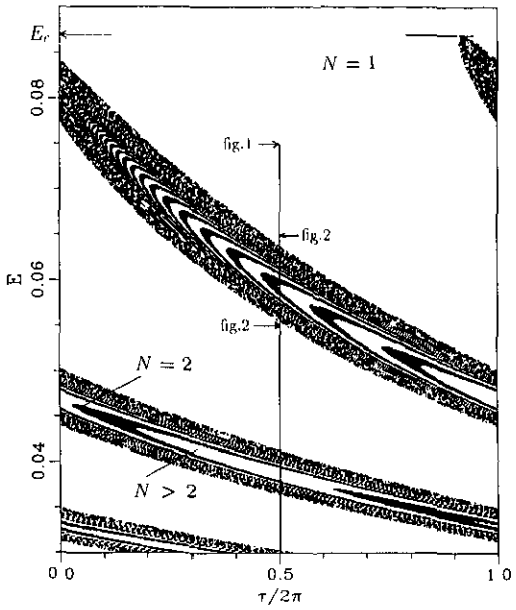

Figure 5. The subset C_1 (black) of the complex scattering region C, i.e. the subset of (E, τ)-values, which lead to scattering trajectories with exactly two zeros. $\epsilon = 0.1$.

As can be seen, there is a critical energy E_c above which only *simple scattering* with $N = 1$ is possible. Below this value a strip of initial conditions begins on which $N \geq 2$ holds for the corresponding trajectories. We call this strip (which consists of several components because of the folding of $\tau \in \mathcal{R}$ into $\tau \in [0, 2\pi)$) the region C of *complex scattering*. In this region the components of C_1 lie in the shape of loops, which accumulate against the boundary of C. Between these loops there are gaps (in the shape of loops themselves) in which $N \geq 3$. The line $\tau = \pi$ shows the interval boundaries of figure 1 and figure 2.

From figures 1–4 we expect that in the gaps between the C_1-loops there are C_2-loops accumulating against the boundaries of enclosing C_1-loops. And between the C_2-loops there are gaps containing C_3-loops and so on. The region of complex scattering has a self-similar structure. If we removed all open $C_1, C_2, \ldots$-loops, a Cantor set of lines consisting of capture orbits and orbits with $E' = 0$ parabolic escape would remain. So we have demonstrated numerically the appearance of chaotic scattering for our example potential.

As we said at the beginning, our example is a representative of a class of potentials, for which the existence of a hyperbolic set, whose dynamics can be described in terms of symbolic dynamics, can be shown analytically. This enables us to compare our results of irregular scattering with the properties of the hyperbolic invariant set of the system. For example, since in every step of the self-similar structure of C we found an infinity of components, on which the scattering map S is continuous, one can expect that the symbolic dynamics of the horseshoe involves an infinite number of symbols. This is true indeed, as will be seen.

The aim of the remaining sections is to find the connection between the hyperbolic invariant set and the chaotic scattering that originates from it. We will try to verify in detail for our class of systems the picture given in the introduction: the scattering singularities are caused by the stable invariant manifolds of the hyperbolic invariant

set, which are transported by means of the Hamiltonian flow of the system into the set of the scattering initial conditions. In this way the fractal properties of the hyperbolic invariant set mirror themselves in the scattering data.

3. The appearance of horseshoe chaos

In this section we want to analyze the formation of horseshoe chaos in our class of systems. Results concerning this problem were found by Alekseev [15–17]. (A review by Alekseev can be found in [18]; a special case—the restricted three-body problem—is discussed by Moser in [20].) We present here a summary of this work because the results are not yet as widely known as they deserve to be with regard to their importance for scattering chaos. This will give us insight into the dynamics of one-dimensional oscillatory potential wells, which we need in order to understand their scattering behaviour. However, the existence of a horseshoe will only be shown locally so that we have to extrapolate it to a global scale. This will be done qualitatively in section 4.

We begin with the introduction of an appropriate discrete map, which allows us to describe the dynamics of the system. If we regard symmetry and attractivity of $V(x,t)$ with respect to $x = 0$, the return map D of our system can be defined as follows. Every time a solution $x(t)$ of (1) crosses the origin $x = 0$ (which has to take place at least once because of the attractivity of the potential), we mark the time t_n and the momentum p_n at this instant. The triple $(x = 0, p_n, t_n)$ uniquely determines an initial condition of (1); we denote the corresponding solution as $x(t; p_n, t_n)$. If we consider a zero (p_n, t_n) of a solution $x(t)$, there are two possibilities for what can happen next: either (i) the particle is reflected by the potential and crosses the origin at time t_{n+1} with momentum p_{n+1} again in the opposite direction, or (ii) the particle is not reflected but escapes to $x = \infty$ or $x = -\infty$. In the first case D is defined as

$$D : (p_n, t_n) \to (p_{n+1}, t_{n+1}). \tag{9}$$

Symmetry and periodicity of $V(x,t)$ yield the identities

$$x(t; p_n, t_n) = x(t + 2\pi; p_n, t_n + 2\pi) = -x(t; -p_n, t_n) \tag{10}$$

which allow us to restrict the variables (p_n, t_n) to the intervals $p_n \geq 0$ and $0 \leq t_n < 2\pi$, respectively. As for $p_n = 0$ we have the trivial solution $x(t) \equiv 0, p(t) \equiv 0$ (which follows from the second identity of (10)) and t_n in this case is undefined; we can interpret (p_n, t_n) as a pair of polar coordinates in a plane Γ. Thus, D can be understood as a map acting on the points of Γ.

The domain R^+ of D is given by all those points $(p_n, t_n) \in \Gamma$ for which the corresponding solution $x(t; p_n, t_n)$ is reflected by the potential and possesses a further zero at time t_{n+1} : $x(t_{n+1}; p_n, t_n) = 0$. This corresponds to case (i). In case (ii) D is not defined. In case (i) let T^+ and X^+ be the time and space coordinate at the instant the particle changes its direction of motion (see figure 6). In case (ii) we define $T^+ = \infty$, $X^+ = \infty$. Then one considers the function

$$E^+(p_n, t_n) = \frac{p^2(T^+)}{2} + V_0(X^+) = \begin{cases} V_0(X^+(p_n, t_n)) & \text{for (i)} \\ E'(p_n, t_n) & \text{for (ii)} \end{cases} \tag{11}$$

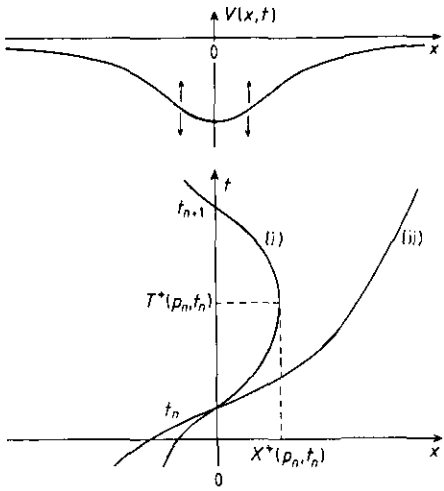

Figure 6. Symmetric oscillating potential well (upper part). Solutions $x(t;p_n,t_n)$ with (i) return and (ii) no return (lower part).

with the time-averaged potential $V_0(x) = (2\pi)^{-1}\int_0^{2\pi} V(x,t)\mathrm{d}t$. Physically, E^+ is the energy of the particle at time T^+ and place X^+ in the time-averaged potential $V_0(x)$. In case (ii) E^+ is equal to the energy E' of the out-asymptote of a scattering process for $t \to +\infty$.

The function $E^+(p_n,t_n)$ has some interesting properties. It is finite and continuous on the whole plane Γ and continuously differentiable on $\Gamma\backslash\{0\}$. The value of its unique minimum in the origin of Γ is $V_0(x=0)$. Its level lines $E^+(p_n,t_n) = \text{constant} > V_0(0)$ are diffeomorph to circles, i.e. they are Jordan curves. This statement will turn out to be useful soon. According to the values of $E^+(p_n,t_n)$ we can subdivide Γ in the following way:

$$\{0\} = \{(p_n,t_n)|E^+(p_n,t_n) = V_0(0)\} \tag{12}$$

$$R^+ = \{(p_n,t_n)|V_0(0) < E^+(p_n,t_n) < 0\} \tag{13}$$

$$P^+ = \{(p_n,t_n)|E^+(p_n,t_n) = E' = 0\} \tag{14}$$

$$H^+ = \{(p_n,t_n)|E^+(p_n,t_n) = E' > 0\}. \tag{15}$$

The origin 0 of Γ corresponds to the trivial solution. R^+ was introduced as the domain of D. This is consistent with the above definition, because the inequality $V_0(0) < E^+(p_n,t_n) < 0$ is equivalent to $0 < X^+(p_n,t_n) < \infty$, which holds in case (i). P^+ is the set of points in Γ corresponding to parabolic solutions. Because of the condition $E^+(p_n,t_n) = 0$ P^+ is a level line of E^+ and therefore a Jordan curve. It encloses the domain R^+ of D, which is an open set and bounded on Γ. The origin lies in the interior of P^+. The elements of H^+, finally, correspond to hyperbolic solutions. For a picture of the situation see figure 7.

All definitions and conclusions for the future $t > t_n$ of a solution $x(t;p_n,t_n)$ can be transferred verbatim into the past $t < t_n$ by following the solution backwards in time. E^- is defined as the energy of the particle in the time-averaged potential $V_0(x)$ at the last turning point X^- at time T^-. In case (i) T^- and X^- are finite and in case (ii) $E^-(p_n,t_n)$ is equal to the energy E of the initial asymptote. Since $E^-(p_n,t_n)$ has

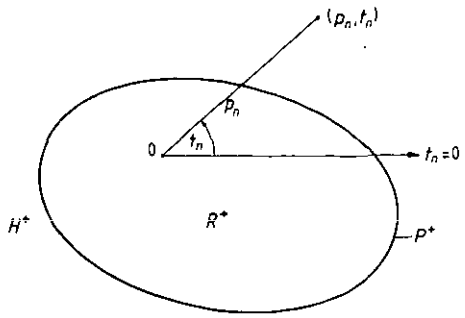

Figure 7. The subsets R^+, P^+ and H^+ of the Γ plane.

the same properties as $E^+(p_n, t_n)$, the sets R^-, P^- and H^- are defined analogously to R^+, P^+ and H^+ and have the equivalent properties and meanings. R^- is the set of all points $(p_n, t_n) \in \Gamma$ for which the particle returns to the origin, if one follows the corresponding solution back to the past $t < t_n$. Thus, R^- is the image of R^+ under the return map D:

$$D(R^+) = R^-. \tag{16}$$

In other words, R^- is the domain of the inverse map D^{-1}. As the return map D is derived from the Hamiltonian system (2), it can be shown to be area preserving. This in addition implies that R^+ and R^- must have the same area. The functions E^+ and E^- are connected by the return map D:

$$E^+ = E^- \circ D. \tag{17}$$

In words this means: the averaged energy of the next turning point of the actual zero is equal to the averaged energy of the last turning point of the next following zero of a solution of (1).

If the potential $V(x,t) = V_0(x)$ is not time dependent, the energy is an integral of motion. Bound motion is then given for energies less than zero, and unbound motion is given for energies greater than or equal to zero. R^+ and R^- coincide in this case and are given by the open circular disc

$$p_0 < \sqrt{-2V_0(0)}. \tag{18}$$

The appearance of chaotic motion in our class of systems results from the fact that $R^+ \neq R^-$ for time-dependent potentials. The model potential (3) is time independent, if $\epsilon = 0$. Then $R^+ = R^-$ is given by (18). If we let ϵ increase continuously, the actual form of R^+ and R^- for $\epsilon > 0$ must evolve from the open disc (18). Since R^+ and R^- have the same area, one expects that their boundaries P^+ and P^- intersect transversally in an even number of points. We call intersection points of P^+ and P^- with distinct tangents *regular points*. Their existence is of central importance for the following discussion.

The simplest situation with two regular points that is realized in our model potential (3), is sketched in figure 8. In addition to the common features of the whole class of systems, there is a reflection symmetry with respect to the ray $t_n = 0$ due to

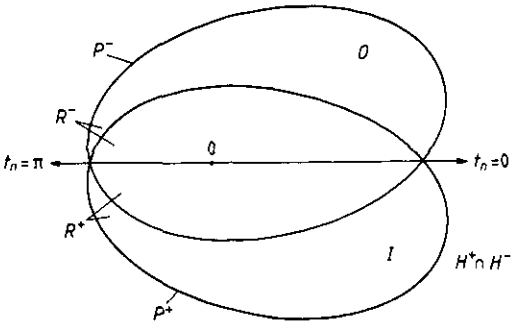

Figure 8. Various sets of initial conditions on Γ as defined in the text. I and O are the incoming and outgoing regions for complex scattering trajectories (see section 4).

time reversal invariance of the potential. The sets I and O marked in figure 8 will be discussed in section 4.

We proceed to a property of the return map which is *essential for the appearance of the horseshoe*. Consider the smooth curve γ in figure 9, which begins in the interior of R^+ and intersects P^+ transversally. In the neighbourhood of the intersection point it meets (due to continuity) all level lines of $E^+(p_n, t_n)$ transversally, too. Due to continuous differentiability of D its image $D(\gamma)$ likewise is a smooth curve. We will try to derive its qualitative shape. For the image point $(p_{n+1}, t_{n+1}) \in D(\gamma)$ of $(p_n, t_n) \in \gamma$ because of (17) the equation $E^-(p_{n+1}, t_{n+1}) = E^+(p_n, t_n)$ has to be fulfilled. That means (p_{n+1}, t_{n+1}) lies as near to the boundary P^- of R^- as (p_n, t_n) lies to the boundary P^+ of R^+. (Remember that $E^-(p_{n+1}, t_{n+1}) = c = E^+(p_n, t_n)$ define level lines of E^- in R^- and of E^+ and R^+ for $c < 0$.) The qualitative shape of $D(\gamma)$ becomes clear, if we also regard the following effect: while we approach P^+ on the curve γ, the time of the next zero t_{n+1} grows to infinity, because for $(p_n, t_n) \in P^+$ the corresponding solution escapes parabolically, i.e. $t_{n+1} = \infty$. Since t_{n+1} is the azimutual angle of the image (p_{n+1}, t_{n+1}), $D(\gamma)$ will wind around the origin an infinite number of times, while it approaches P^- asymptotically. We conclude that $D(\gamma)$ is an infinite spiral asymptotic to the boundary P^-.

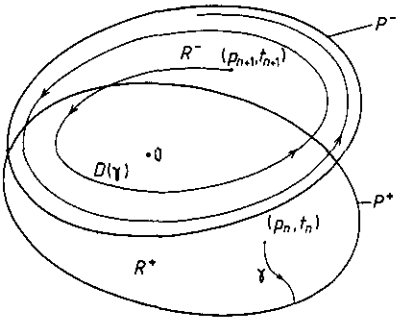

Figure 9. Image $D(\gamma)$ of a curve γ meeting P^+ transversally.

Now we are prepared to show how a horseshoe arises in the dynamics of the return map. We consider the neighbourhoods U_1 and U_2 of the two regular points which are defined by the conditions $|E^-(p_n, t_n)| \leq \delta$ and $|E^+(p_n, t_n)| \leq \delta$. The boundaries

of U_1 and U_2 are given by corresponding pieces of the level lines $E^-(p_n,t_n) = \pm\delta$ and $E^+(p_n,t_n) = \pm\delta$ (see figure 10). The boundaries $E^-(p_n,t_n) = \pm\delta$ of $U_1 \cap R^+$ are smooth curves beginning in the interior of R^+ and intersecting P^+ transversally. Consequently, as described above, by application of D they are mapped to infinite spirals approaching the boundary P^- asymptotically. Since $D(U_1 \cap R^+)$ is bounded by these spirals, it must have the shape indicated in figure 10. As is also indicated in figure 10, the image $D(U_1 \cap R^+)$ intersects U_1 as well as U_2 in an infinite number of strips accumulating against P^-. This of course is true for $D(U_2 \cap R^+)$, too, so that one finds in $U_1 \cap R^-$ and $U_2 \cap R^-$ strips coming from $U_1 \cap R^+$ as well as from $U_2 \cap R^+$.

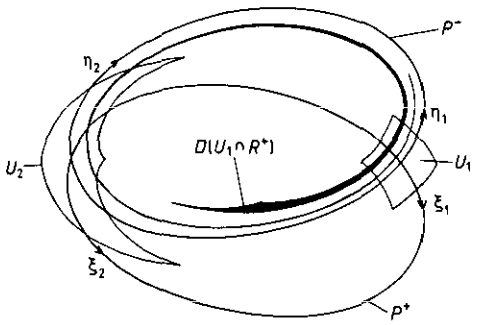

Figure 10. The neighbourhoods U_1 and U_2 of the two regular points. Image of $U_1 \cap R^+$ under D.

If we apply the coordinate transformation

$$(p_n,t_n) \to (\xi_i,\eta_i) = (E^-(p_n,t_n), E^+(p_n,t_n)) \qquad i = 1,2 \tag{19}$$

for the neighbourhoods U_1 and U_2, they will take on the shape of squares

$$Q_i = \{(\xi_i,\eta_i) | |\xi_i| \le \delta, |\eta_i| \le \delta\} \qquad i = 1,2. \tag{20}$$

For the following it is useful to call the ξ_i directions of the squares horizontal and the η_i directions vertical. The return map D on the squares can also be represented by the coordinates ξ_i and η_i. To show how D acts on the squares Q_i $(i = 1,2)$ that are depicted in figure 11, we also sketch schematically their pre-images $D^{-1}(Q_i \cap R^-)$ and images $D(Q_i \cap R^+)$ (compare with figure 10). The pre-images intersect Q_i $(i = 1,2)$ in an infinite number of horizontal strips accumulating against the ξ_i axes, whereas the images intersect Q_i $(i = 1,2)$ in an infinite number of vertical strips accumulating against the η_i axes. We supply the horizontal strips a_{ij} with two indices i and j following the rule: i marks the square Q_i in which the strip a_{ij} lies and j counts (in the η_i direction) the strips lying in Q_i. By the application of D each horizontal strip a_{ij} is mapped to a vertical strip b_{ij} which is part of the intersection of $D(Q_i \cap R^+)$ with the square $Q_{i'}$. So the b_{ij} take their index from their pre-image a_{ij} but lie in the square $Q_{i'}$:

$$D(a_{ij}) = b_{ij} \subset Q_{i'}. \tag{21}$$

In figure 11 we have the rule: $i' = i$, if $j = 1,3,5,\ldots$ and $i' \neq i$, if $j = 2,4,6,\ldots$. The image strip b_{ij} evolves from its pre-image strip a_{ij} by contracting a_{ij} in the horizontal

direction, by expanding it in the vertical direction and by moving it along the spiral from the square Q_i to the square $Q_{i'}$. In this procedure the vertical edges of a_{ij} are mapped onto the vertical edges of b_{ij} and the same is true for the horizontal edges. These properties, namely (i) contraction in the horizontal direction, (ii) expansion in the vertical direction and (iii) the way the horizontal and vertical boundaries of horizontal strips are mapped, define a generalized horseshoe map (see [22,23]).

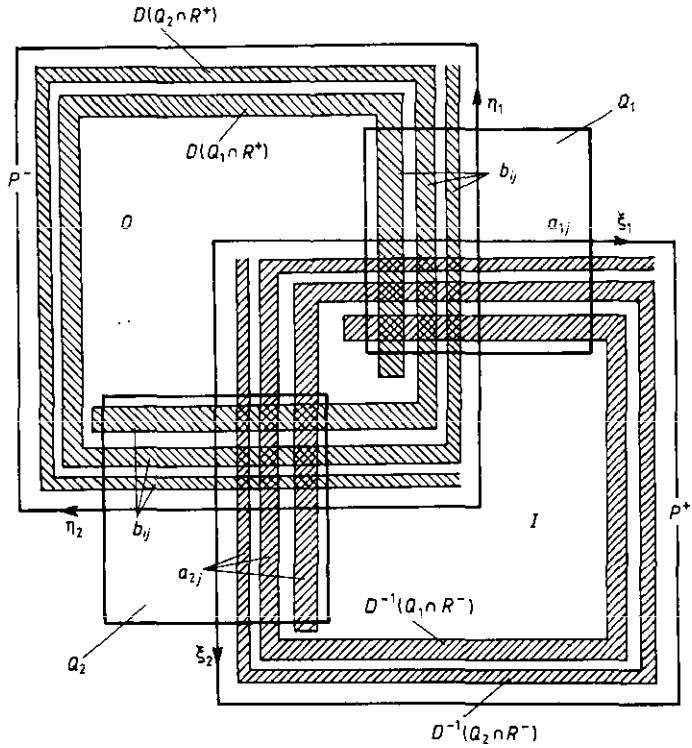

Figure 11. Schematic plot of $D(Q \cap R^+)$ and $D^{-1}(Q \cap R^-)$ with $Q = Q_1 \cap Q_2$. Horizontal strips a_{ij} and vertical strips b_{ij}.

The main consequence of the horseshoe is the existence of a hyperbolic set Λ, which is invariant under D on $Q = Q_1 \cup Q_2$. The dynamics of D is topologically conjugate to the shift map σ on the space Σ of sequences s. Σ is given by

$$\Sigma = \{s = (\ldots s_{-2}s_{-1}; s_0 s_1 s_2 \ldots) | s_k \in A \forall k \in \mathcal{Z}\}. \tag{22}$$

The alphabet A, from which the elements of the sequences are taken, consists of the indices marking the horizontal strips. So in our case we have $A = \{1,2\} \times \mathcal{N}$. This confirms the impression we had from the scattering data in section 1: in our system an infinite alphabet is needed for the horseshoe. The shift map σ shifts all elements of a sequence one place to the left:

$$\sigma : \Sigma \to \Sigma, s' = \sigma(s) \qquad \text{with} \qquad s'_k = s_{k+1} \forall k \in \mathcal{Z}. \tag{23}$$

The conjugacy of D and σ is given by a homeomorphism ϕ and is usually expressed

in the following commutative diagram:

$$\begin{array}{ccc} \Lambda & \xrightarrow{D} & \Lambda \\ \phi \downarrow & & \downarrow \phi \\ \Sigma & \xrightarrow{\sigma} & \Sigma \end{array} \tag{24}$$

ϕ assigns to each point $q \in \Lambda$ a sequence $s \in \Sigma$ by the following rule: the kth symbol s_k of s takes on the value $r \in A$, if the kth iterate $D^k(q)$ lies in the horizontal strip a_r. Thus, the sequences s contain the information about the dynamics of the corresponding point q under iteration. Concerning the construction of the space of sequences in our system we have to pay attention to a subtlety, that was overlooked by Alekseev ([17, 18]). Not all sequences $s \in \Sigma$ are allowed. As already mentioned in connection with (21) one deduces from figure 11 that an order $\ldots s_k s_{k+1} \ldots$ is forbidden unless $i_{k+1} = i_k$ for $j_k = 1, 3, 5, \ldots$ or $i_{k+1} \neq i_k$ for $j_k = 2, 4, 6, \ldots$, i.e.

$$i_{k+1} + i_k + j_k = \text{ odd integer.} \tag{25}$$

Consequently in (24) Σ has to be replaced by the restricted space of sequences

$$\Sigma' = \{s | s_k \in \{1, 2\} \times \mathcal{N}, (25) \text{ fulfilled } \forall k \in \mathcal{Z}\}. \tag{26}$$

The transition matrix (see [23]) of Σ' is irreducible. As a consequence the set Σ', if equipped with an appropriate metric, is totally disconnected and perfect but not compact due to the infinity of symbols. These properties are transferred to the set Λ by ϕ^{-1}. Thus, Λ is a non-compact 'Cantor set' (bounded on Q but not closed).

So far we were concerned with the symbolic dynamics as commonly known. In our system it is possible to extend Σ' to a space of sequences Σ^+ which in addition to the bi-infinite sequences of Σ' contains sequences that are finite to one or both sides. To establish a conjugacy as in (24) the invariant set Λ must also be extended to a set Λ^+ which contains the points of Q having the corresponding finite dynamics under forward or backward iteration of D. The 'entrances' or 'exits' of such sequences correspond to scattering motion for $t \to -\infty$ or $t \to +\infty$, respectively.

Let $D^k(q) \in Q_{i_k}$ $(k \in \mathcal{Z})$. We consider as *entrance* the vertical line $\xi_{i_k} = E \geq 0$. If $D^k(q)$ lies on an entrance, it must be the first iterate of q, because $\xi_{i_k} = E^-(D^k(q)) \geq 0$ means that $D^k(q) \in P^- \cup H^-$ (remember the definitions of $R^\pm$, $P^\pm$, $H^\pm$). One can regard an entrance as a degenerate vertical strip. By the declaration of the initial energy E and the following dynamics the corresponding point $q \in Q$ is defined uniquely. We mark the opening element of such a sequence by $s_{k-1} = E$. $D^k(q)$ lies in the horizontal strip a_{s_k} which defines the next element. Thus, the corresponding sequence looks like $(Es_k \ldots s_{-1}; s_0 \ldots)$. As an *exit* we characterize the horizontal line $\eta_{i_k} = E' \geq 0$ that one can regard as a degenerate horizontal strip. If $D^k(q)$ lies on an exit, it is an element of $P^+ \cup H^+$, because $E^+(D^k(q)) \geq 0$ holds. Consequently $D^k(q)$ must be the last zero of the trajectory corresponding to $q \in Q$. As the closing element of the sequence we take $s_k = (i_k E')$. The corresponding sequence $(\ldots s_{-1}; s_0 \ldots s_{k-1}(i_k E'))$ also uniquely defines a point $q \in Q$. (We remark that there

is a slight asymmetry in specifying opening elements and closing elements. As an exit replaces a horizontal strip one has to name the square Q_{i_k} in which it lies. For an entrance replacing a vertical strip this is not necessary, because the square of the first zero is marked by the subsequent element of the sequence.)

One can also construct sequences that are finite to both sides. As can be shown, they are also in one-to-one correspondence to points in $q \in Q$. If we extend the alphabet A with the help of the set $B = [0, \delta]$ of opening symbols and the set $C = \{1, 2\} \times [0, \delta]$ of closing symbols, we can write the extended space of sequences as

$$\Sigma^+ = \{s | s_k \in A \cup B \cup C, \text{ but } s_m \notin B \text{ for } m \geq 0 \text{ and } s_n \notin C \text{ for } n \leq 0, (25) \text{ fulfilled } \forall k \in \mathcal{Z})\}. \tag{27}$$

The shortest possible sequences in Σ^+ are of the form $(E; s_0(i_1 E'))$. The shift map σ can be applied to the elements of Σ^+ at least once. The image of Σ^+ is the set Σ^- consisting of all sequences that can be generated by shifting the sequences of Σ^+ one place to the left.

We are especially interested in what Λ^+ looks like. We give an inductive construction. Consider an arbitrary horizontal strip a_{s_0}. If we map it by the application of D to its image b_{s_0} lying in Q_{i_1} the upper half of b_{s_0} will lie on the upper half ($\eta_{i_1} \geq 0$) of the square Q_{i_1}. So a_{s_0} contains an η substrip (of order 0) which consists of points having exactly one further iterate. In the other half of a_{s_0} there are horizontal substrips $a_{s_0 s_1}$ containing all the points having at least two further zeros. They accumulate against the edge of the η substrip of order 0, which belongs to the parabolic escape $E' = 0$. Two successive applications of D map them to the vertical strips b_{s_1} (lying in Q_{i_2}). The upper half of them lies in the area $\eta_{i_2} \geq 0$. Consequently the strips $a_{s_0 s_1}$ all have η substrips (of order 1) consisting of points having exactly two further iterates. The other half of $a_{s_0 s_1}$ contains substrips $a_{s_0 s_1 s_2 \ldots}$ and so on. We are led to a self-similar structure, which strongly reminds us of the one we found by the computation of the scattering map. In figure 12 the horizontal strips $a_{s_0 s_1 \ldots s_{l-1}}$ of order $l - 1$ are shown. They contain the η substrips of order $l - 1$ (hatched) and in the other half a group of horizontal strips of order l. They converge against the edge of the η_{l-1} continuum corresponding to solutions escaping with energy $E' = 0$ after $N = l$ further zeros.

The same construction can be carried out for the vertical strips $b_{s_{-1}}$ lying in Q_{i_0} with respect to backward iteration $s_{-1} s_{-2} s_{-3} \ldots$. One obtains the same picture in the half $\xi_{s_0} < 0$ of Q_{i_0}. The intersection of all η_l and, say ξ_m substrips, constitutes Λ^+. One can show that ϕ is a homeomorphism on Λ^+, too. Defining $\Lambda^- = D(\Lambda^+)$, for our system the extended commutative diagram

$$\begin{array}{ccc} \Lambda^+ & \xrightarrow{D} & \Lambda^- \\ \phi \downarrow & & \downarrow \phi \\ \Sigma^+ & \xrightarrow{\sigma} & \Sigma^- \end{array} \tag{28}$$

We presume that the compactification of Λ to a Cantor set is accomplished by adding parabolic motion for $t \to -\infty$ ($E = 0$) and $t \to +\infty$ ($E' = 0$). To Σ' one adds the sequences beginning with $E = 0$ and ending with $(i_n E')$ with $E' = 0$. The

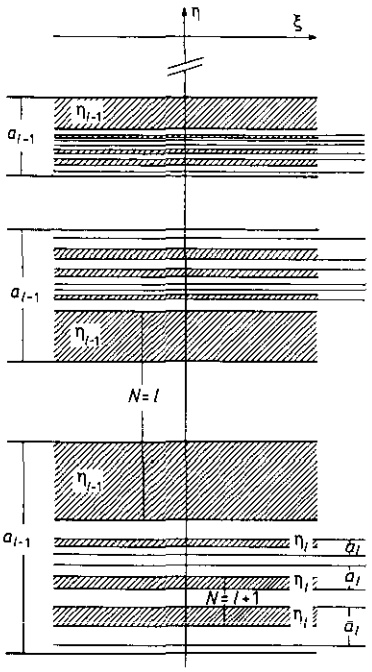

Figure 12. Horizontal strips and η substrips of orders l, $l-1$: a_l, a_{l-1} and η_l, η_{l-1}, respectively.

proof of this statement goes beyond the scope of this paper. It might be a subject of interest for further investigation.

What are our results? We have shown locally—i.e. in small neighbourhoods of the regular points—that the return map D contains a horseshoe with an infinite alphabet. We succeeded in extending Σ and Λ so that scattering motion also can be described. The conjugacy (28) leads to the following important result. Given any initial and final energies E, E' (sufficiently small) and any sequence $s_m \dots s_{-1} s_0 \dots s_n$ ($m < 0$, $n > 0$) which is allowed by (25) there is exactly one scattering trajectory, which comes in with energy E, goes out with energy E' and has the intermediate dynamics $s_m \dots s_{-1} s_0 \dots s_n$. The existence of capture and decay motion is guaranteed by the corresponding sequences of Σ^+.

4. Scattering data and internal dynamics

From section 3 we know that there is a horseshoe in the dynamics of the return map and we are sure of the existence of capture, decay and scattering motion with arbitrary internal dynamics. Constructing the set Λ^+ we obtained a picture, that strongly reminds us of the structure of our scattering data (see figure 12). The deficiency of these results is their restriction to small neighbourhoods of the two regular points. We will try to improve the situation by some global qualitative considerations. To explain the scattering data by means of the dynamics of the return map D on the plane Γ we must in addition find out in which way the points on Γ are connected with the initial and final states of scattering characterized by the points in the (E, τ) plane. Together with our global considerations this will enable us to understand the fractal structure

of the region of complex scattering C we observed in the plane of scattering initial conditions.

To begin with, we define the sets

$$I = (P^- \cup H^-) \cap R^+ \qquad \text{and} \qquad O = R^- \cap (P^+ \cup H^+) \tag{29}$$

which are of central importance for scattering in our class of systems (look back at figure 8). The elements of I lie in the domain of D and in the complement of the domain of D^{-1}. That means $(p_0, t_0) \in I$ is the zero of a solution $x(t; p_0, t_0)$ which has no further zero in the past $t < t_0$, but at least one further zero $(p_1, t_1) \in R^-$ in the future $t > t_0$. Whether there is a third zero (p_2, t_2) of $x(t; p_0, t_0)$ depends on where (p_1, t_1) lies: if it is an element of $R^+ \cap R^-$, a further zero (p_2, t_2) exists; but if it is an element of O, (p_1, t_1) is the last zero of $x(t; p_0, t_0)$. Generally, in the nth step one must know whether (p_n, t_n) lies in $R^+ \cap R^-$ or O to decide if there is a further zero (p_{n+1}, t_{n+1}) or not. Thus, I and O have a complementary meaning: I, the incoming region, serves as an *entrance* from the asymptotic region to the internal dynamics of the system described by means of the return map D, and O, the outcoming region, is the *exit* back to the asymptotic region.

We claim that I corresponds to the region of complex scattering C (see section 2) in the (E, τ) plane. The scattering initial states in C belong to solutions with two or more zeros ($N \geq 2$). Outside C we only found simple scattering ($N = 1$) in section 2. The zeros in I likewise belong to solutions with at least two zeros, and I is a subset of $P^- \cup H^-$ which contains all scattering initial conditions in Γ. The complement of I in $P^- \cup H^-$ is $(P^- \cup H^-) \cap (P^+ \cup H^+)$ which corresponds to solutions having exactly one zero (simple scattering, $N = 1$). The transformation from a zero $(p_0, t_0) \in P^- \cup H^-$ to a scattering initial condition (E, τ) is given by

$$(E, \tau) = \chi(p_0, t_0) = \lim_{t \to -\infty} T_t \circ \Phi_{tt_0}(x_0 = 0, p_0). \tag{30}$$

The Hamiltonian flow Φ_{tt_0} of the system maps the initial condition $x(t_0) = 0$, $p(t_0) = p_0$, corresponding to the zero $(p_0, t_0) \in P^- \cup H^-$, backwards in time to the point $(x(t), p(t))$ in phase space. The corresponding asymptote (E, τ) is then determined by the subsequent application of T_t in the limit $t \to -\infty$. χ maps the level line $E^-(p_0, t_0) = \text{constant}$, which surrounds R^- in Γ, to the horizontal line $E = \text{constant}$ in the (E, τ) plane. In particular P^- corresponds to $E = 0$. The behaviour of χ is determined by the following two asymptotic properties due to the definition of τ in (4). Let $t_0 \in [0, 2\pi)$. (i) For $E \to 0$ we have $\tau \to \infty$. (ii) For $E \to \infty$ we have $\tau \to t_0$.

I is seperated from simple scattering in $P^- \cup H^-$ by the intersection of P^+ with $P^- \cup H^-$ (see figure 8). The boundary of C in the (E, τ) plane is the image of $P^+ \cap (P^- \cup H^-)$ under χ. The critical energy E_c, the upper bound for complex scattering to take place, is given by the highest level line $E^-(p_0, t_0) = \text{constant}$ which is intersected by $P^+ \cap (P^- \cup H^-)$. We confirm our considerations by a numerical experiment on example (3). We computed $P^+ \cap (P^- \cup H^-)$ for several values of ϵ and transferred it by numerical integration into the (E, τ) plane. The results can be seen in figure 13. As one expects from property (i), C possesses an infinite 'tail' for $\tau \to \infty$ as $E \to 0$. We observe that E_c and the area of C increase with increasing values of ϵ. This is in accordance with the fact that ϵ gives the maximum variation of $V(x, t)$ with time at the origin $x = 0$. ϵ can be shown to be the upper bound for E_c. For our example E_c is almost linearly dependent on ϵ with a factor 0.86. E_c corresponds to

a minimum time interval Δt for traversing the range Δx of the potential. As a lower bound for Δt one estimates (with $E_c < \epsilon$)

$$\Delta t = \frac{\Delta x}{\sqrt{2E_c}} > \frac{\Delta x}{\sqrt{2\epsilon}}. \tag{31}$$

If we estimate Δx as $\sqrt{2}$ (e.g. distance of turning points of (3)), we get $\Delta t > \epsilon^{-1/2}$, which is a considerable fraction of the period of oscillation $T = 2\pi$ for the ϵ values of figure 12.

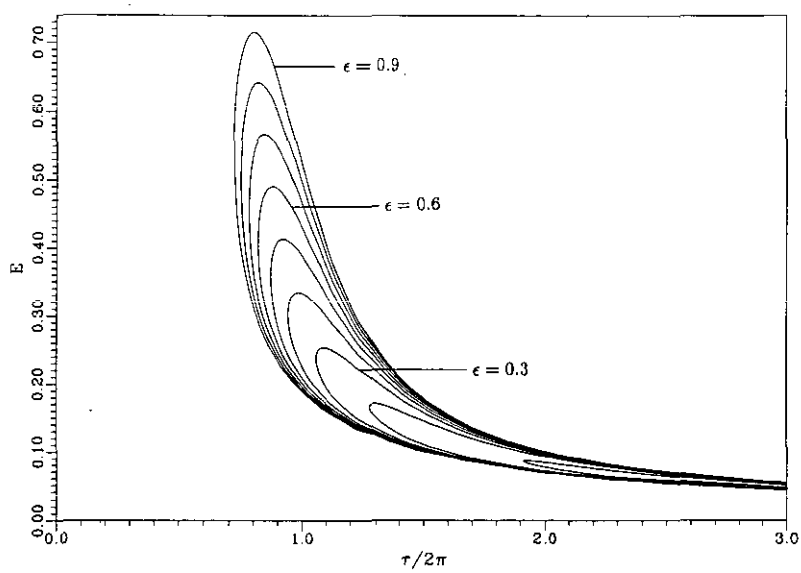

Figure 13. Regions C of complex scattering by the oscillating potential well (3) $\epsilon = 0.1, 0.2, \ldots, 0.9$.

We return to the fractal properties of C. We want to explain the fractal organization of the sets C_n corresponding to solutions with $N = n + 1$ zeros. By means of χ this problem is now reduced to the investigation of I. We can carry out this investigation because of the detailed knowledge we have of the properties of the return map D. We begin with the definition of the sets

$$S_n^+ = \{(p_0, t_0) | D^k(p_0, t_0) \in R^+ \quad \text{for} \quad k = 0, 1, \ldots, n-1 \quad \text{and} \quad D^n(p_0, t_0) \in O\} \tag{32}$$

$n = 1, 2, 3, \ldots$ (D^0 the identity). The elements (p_0, t_0) of S_n^+ in Γ correspond to solutions having n zeros in the future $t > t_0$ apart from the zero (p_0, t_0) and then escape to a final state of scattering. The sets

$$I_n = I \cap S_n^+ \tag{33}$$

correspond (via χ) to the sets C_n of C. The intersection of S_n^+ with I guarantees that (p_0, t_0) is the first zero of a solution in I_n. So the total number of zeros for elements of I_n is $N = n + 1$. By means of the commutative diagram (28) one can deduce from the sequences $(E; s_0 s_1 \ldots s_{n-1}(i_n E'))$ that none of these sets is empty. But $I_1, I_2, I_3, \ldots$

do not contain all points of I. There are the sequences $(E; s_0 s_1 s_2 \ldots)$ with an infinite number of zeros for $t > t_0$. They correspond to capture orbits. Thus we conclude that the set

$$I_\infty = I \setminus \bigcup_{n=1}^{\infty} I_n \tag{34}$$

likewise is non-empty. Its image C_∞ under χ represents the set of scattering singularities of the scattering map S. It consists of the stable manifolds of Λ.

We want to deduce the shape of I_n and I_∞ now. For this aim we construct the sets S_n^+ (see figure 14). We obtain S_1^+ according to its definition as the pre-image of O:

$$S_1^+ = D^{-1}(O). \tag{35}$$

To find its shape we remember that a curve γ, intersecting P^+ transversally from its interior R^+, is mapped by D onto an infinite spiral asymptotic to P^-. The same holds for the application of D^{-1} to a curve intersecting P^- transversally from its interior R^-. Then the pre-image is an infinite spiral in R^+ converging against P^+. The boundary between O and $R^- \cap R^+$ intersects P^- transversally at the two regular points. Thus, the pre-images of these two ends of the boundary represent such spirals as described above. As a consequence S_1^+ qualitatively has the shape indicated in figure 14. The complement of S_1^+ in R^+ is given by the pre-image $D^{-1}(R^+ \cap R^-)$. Now the shape of $I_1 = I \cap S_1^+$ can easily be read off. I_1 consists of an infinite number of spiral segments accumulating against P^+. Transporting this shape back into the (E, τ) plane with the help of χ we find the picture given in figure 5 in which C_1 was calculated numerically.

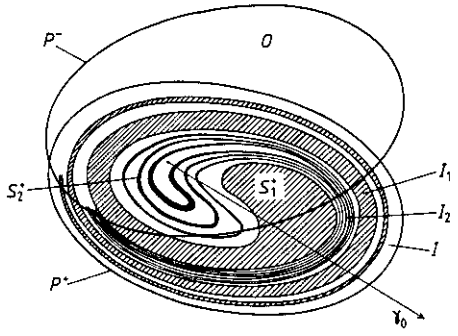

Figure 14. Subsets S_n^+ and $I_n = I \cap S_n^+$ for $n = 1, 2$. The I_n are intersected by the ray γ_0. See figure 15.

We continue with the construction of S_2^+ from S_1^+ in the following way:

$$S_2^+ = D^{-1}(S_1^+ \cap R^-). \tag{36}$$

Since $S_1^+ \cap R^-$ is a subset of $R^+ \cap R^-$, the set S_2^+ lies in $D^{-1}(R^+ \cap R^-)$, which is the complement of $D^{-1}(O)$ on R^+. $S_1^+ \cap R^-$ essentially consists of an infinity of segments meeting P^+ transversally on both ends and accumulating at P^-. Each of these segments is mapped under D^{-1} to a loop with two infinite tails spiralling against

P^+. The set S_2^+ is constituted by all these double spirals; it is also sketched in figure 14. As a consequence $I_2 = I \cap S_2^+$, i.e. the set of points belonging to scattering orbits with three zeros, consists of an infinity of segments between each pair of neighbouring I_1 segments accumulating at the boundaries of the I_1 segments.

The structure given above continues in a self-similar way: between each pair of I_n segments there is an infinity of I_{n+1} segments accumulating against the I_n boundaries. This can be shown by making use of the generalization of (36):

$$S_{n+1}^+ = D^{-1}(S_n^+ \cap R^-) \tag{37}$$

for $n = 1, 2, 3, \ldots$. The segments $I_1, I_2, \ldots$ are transported by χ to the corresponding loops of $C_1, C_2, \ldots$ under conservation of their accumulation structure. To see what happens if one makes a section of C—as we did in figures 1–4 by setting $\tau = \pi$—we have also plotted a ray γ_0 in figure 15 which has a non-empty intersection with I. The structure of the intersections $I_1 \cap \gamma_0$, $I_2 \cap \gamma_0$ and $I_3 \cap \gamma_0$ is sketched in figure 15. We find infinities of accumulating intervals, as we computed numerically in figure 1–4. (The section $t_0 =$ constant is not exactly the same as $\tau =$ constant, but a qualitative difference can only be seen for I_1 and C_1 intervals.)

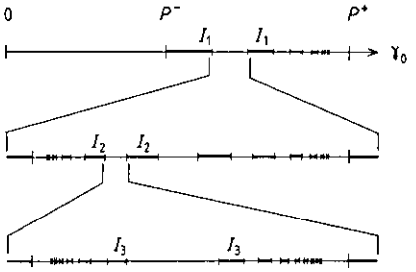

Figure 15. Selfsimilar distribution of the intervals $I_n \cap \gamma_0$.

Finally we want to add something about the stable invariant manifolds of Λ. We describe the situation in I. The results can be transferred via χ to the region of complex scattering C. The stable invariant manifolds of Λ (see section 3) are given by all the points in Λ^+ corresponding to sequences

$$(E; s_0 s_1 s_2 \ldots) \tag{38}$$

that are finite to the left, but have infinite dynamics to the right. One can show that the infinite forward sequence $s_0 s_1 s_2 s_3 \ldots$ in Q_{i_0} fixes a horizontal curve that is a stable manifold of Λ (see [22, 23]). Thus, each allowed forward dynamics determines one stable manifold of Λ. The point belonging to the sequence (38) is determined by the intersection of the horizontal stable manifold with the vertical line $\xi_{i_0} = E$. So the stable manifolds are horizontal lines in $Q_1 \cap I$ and $Q_2 \cap I$. This means that they are parallel to P^+ in the vicinity of the two regular points.

This is in accordance with our global considerations. We obtain the stable manifolds globally by removing all the sets I_n successively (see equation (34)). I_∞ consists of the uncountable number of curves lying between $I_1, I_2, I_3, \ldots$ (parallel to P^+). This set is fractal, but not closed. Its closure is accomplished through the addition of all the solutions which in the future escape after an intermediate dynamics $s_0 s_1 s_2 \ldots s_n$ parabolically with $E' = 0$. The fractal I_∞ with its closure forms a Cantor set consisting of an uncountable number of lines. In physical terms, the Cantor set of discontinuities of the scattering map is caused by capture orbits and orbits with parabolic escape.

5. Conclusions

The return map that we introduced in section 3 with the help of a somewhat unusual surface of section turned out to be a very useful tool for the understanding of irregular scattering in the considered class of systems. This is due to the following two properties of the chosen surface of section. Firstly, the spiral-property of the return map, which is essential for the appearance of a horseshoe, enabled us to construct the sets I_n (corresponding to solutions with $N = n+1$ zeros) in the incoming region I. Secondly, the subset H^- of Γ is in one-to-one correspondence with the initial states of scattering motion by means of the transformation χ. The region C of complex scattering in the (E, τ) plane, which we found numerically in section 2, is the image of $I \subset H^-$ under χ. Thus, the fractal structure in the interior of I explains the one we found numerically in the interior of C.

The level of the self-similar structure in I and C is controlled by the number N of zeros of the solutions, i.e. the number of times a solution passes through the surface of section $x = 0$. The higher N, the longer a trajectory follows the dynamics of the hyperbolic invariant set Λ. As it seems from our numerical experiments, the measure of the sets I_n and C_n decreases geometrically with increasing $n = N - 1$. The capture orbits constituting I_∞ and C_∞ consequently have measure zero in the (E, τ) plane. It would be an interesting subject of further investigation to analyze the fractal properties of C_∞: e.g. the fractal dimension, the scaling function or the distribution of Lyapunov exponents of bounded orbits. These quantities were computed in [13] for the simpler problem of scattering off three hard discs.

We believe that the numerical results of irregular scattering we obtained for our example potential can be transferred to the whole class of potentials. This holds, because the properties we used for the considerations in section 4 are valid for the whole class of potentials. But, eventually, slight alterations may be neccessary. If, for example, there are four regular points, the incoming region I and consequently C will consist of two components which are not connected with each other. This case may appear if one replaces $\cos t$ in the potential (3) by a Fourier series in which the term $\cos 2t$ has a dominant weight.

Finally, we remark that there is always a set in Γ corresponding to bounded motion (this was not regarded in figure 14). Its existence follows from the KAM theorem for ϵ small enough in (3). Around the origin of Γ, which is an elliptic fixpoint, one finds the usual KAM scenario with invariant curves (preserved under perturbation) and stochastic layers in between. There is no transition between the bounded motion inside of these invariant curves and the unbounded motion of Λ.

References

[1] Eckhardt B 1988 *Physica* **33D** 89–98
[2] Rankin C C and Miller W H 1971 *J.Chem.Phys.* **55** 3150–6
[3] Gottdiener L 1975 *Molec. Phys.* **29** 1585–95
[4] Noid D W, Gray S K and Rice S A 1986 *J.Chem.Phys.* **84** 2649–52
[5] Jung C 1986 *J. Phys. A: Math. Gen.* **19** 1345–53
[6] Eckhardt B and Jung C 1986 *J. Phys. A: Math. Gen.* **19** L829–33
[7] Jung C 1987 *J. Phys. A: Math. Gen.* **20** 1719–31
[8] Jung C and Scholz H J 1987 *J. Phys. A: Math. Gen.* **20** 3607–17
[9] Petit J M and Hénon M 1986 *Icarus* **66** 536–55
[10] Manakov S V and Shchur L N 1983 *Sov. Phys. JETP Lett.* **37** 54–8

[11] Eckhardt B and Aref H 1988 *Phil. Trans. R. Soc. A* **326** 655—96
[12] Jung C and Scholz H J 1988 *J. Phys. A: Math. Gen.* **21** 2301—11
[13] Eckhardt B 1987 *J. Phys. A: Math. Gen.* **20** 5971—9
[14] Hénon M 1988 *Physica* **33** D 132–56
[15] Alekseev V M 1968 *Math. USSR Sbornik* **5** 73–128
[16] Alekseev V M 1968 *Math. USSR Sbornik* **6** 505–60
[17] Alekseev V M *Math. USSR Sbornik* **7** 1–43
[18] Alekseev V M 1981 *Amer. Math. Soc. Transl.* **116** 97–169
[19] Sitnikov K *Sov. Phys. Dokl.* **5** 647–50
[20] Moser J 1973 *Stable and Random Motions in Dynamical Systems* (Princeton, NJ: Princeton University Press)
[21] Narnhofer H and Thirring W 1981 2 *Phys. Rev. A* **23** 1688–97
[22] Guckenheimer J and Holmes P 1983 *Nonlinear Oscillations, Dynamical Systems, and Bifurcations of Vector Fields* (New York: Springer)
[23] Wiggins S *Global Bifurcations and Chaos* (New York: Springer)